RSC Advances

Check for updates

A hydrothermal synthesis of Ru-doped LiMn$_{1.5}$Ni$_{0.5}$O$_4$ cathode materials for enhanced electrochemical performance

Dengfeng Zhou, [ab] Junqi Li, [*a] Can Chen, [a] Fangchang Lin, [a] Hongming Wu [cd] and Jianbing Guo [ID] [*ac]

An Ru-doped spinel-structured LiNi$_{0.5}$Mn$_{1.5}$O$_4$ (LNMO) cathode has been prepared *via* a simple hydrothermal synthesis method. The as-prepared cathode is characterized *via* Fourier transform infrared (FTIR) spectroscopy, powder X-ray diffraction (XRD), scanning electron microscopy (SEM), laser particle size distribution analysis, X-ray photoelectron spectroscopy (XPS) and electrochemistry performance tests. The FTIR spectroscopy and XRD analyses show that the Ru-doped LNMO has a good crystallinity with a disordered *Fd$\bar{3}$m* space group structure. The disordered structure in the cathode increased and the Li$_x$Ni$_{1-x}$O impurity phase decreased when Ru addition increased. SEM shows that all samples are octahedral particles with homogeneous sizes distribution, and the particle size analysis shows that the Ru-doped samples have smaller particle size. XPS confirms the existence of Ru ions in the sample, and reveals that the Ru induce to part of Mn^{4+} transfers to Mn^{3+} in the LNMO. The electrochemical property indicated that the Ru-doped cathode exhibits better electrochemical properties in terms of discharge capacity, cycle stability and rate performance. At a current density of 50 mA g^{-1}, the discharge specific capacity of the Ru-4 sample is 140 mA h g^{-1}, which is much higher than that of the other samples. It can be seen from the rate capacity curves that the Ru-doped samples exhibit high discharge specific capacity, particularly at high current density.

1. Introduction

Since Sony developed the first commercial lithium battery in 1991, lithium batteries have been used in different commercial electrical products.[1–4] The development of high energy density and low-cost lithium-ion batteries is one of the research hotspots. The cathode material is an essential component of lithium-ion batteries and has a great influence on the capacity and operating voltage of the battery. Therefore, it is very important for the research and exploration of cathode materials.[5–8] The main cathode materials used in lithium-ion batteries include the layer structure (LiCoO$_2$), spinel structure (LiNi$_{0.5}$Mn$_{1.5}$O$_4$) and olivine structure (LiFePO$_4$).[9] The earliest commercial cathode material for lithium-ion secondary batteries is LiCoO$_2$ with a layered structure, which is beneficial for the diffused Li$^+$ ions in the 2D diffusion channel of the CoO$_2$

layer.[10] Nonetheless, a series of problems have appeared in the LiCoO$_2$ cathode. For example, all Li ions cannot undergo a reversible intercalation/de-intercalation reaction due to their own structure. In particular, after numerous times of charging/discharging processes, its crystal structure will undergo changes and its capacity will be reduced, resulting in the decline of its cycling performance. Moreover, cobalt is expensive and toxic.[11,12] Therefore, it is necessary to explore new cathode materials with high energy density, power density, and suitable price and stable properties. Compared to LiCoO$_2$, the LiNi$_{0.5}$Mn$_{1.5}$O$_4$ cathode has a higher operating voltage of 4.7 V, higher than LiCoO$_2$ (3.7 V). The LiNi$_{0.5}$Mn$_{1.5}$O$_4$ cathode also has a higher energy density (~658 W h kg^{-1}).[13] The spinel LiNi$_{0.5}$Mn$_{1.5}$O$_4$ cathode material is considered one of the most promising cathode materials for lithium-ion batteries.

The spinel LiNi$_{0.5}$Mn$_{1.5}$O$_4$ cathode material with the *Fd$\bar{3}$m* space group is fit for Li$^+$ diffusion.[14,15] Lithium-ion can be diffused along the (011), (101), and (110) directions creating a 3D Li$^+$-diffused channel. This character makes it easy to obtain high power density.[13,16] The problem with the LiNi$_{0.5}$Mn$_{1.5}$O$_4$ cathode is that it will have a series of side reactions with the electrolyte at high voltages (~5 V), which will reduce the cycle life and safety of the battery. Therefore, it is necessary to modify the LiNi$_{0.5}$Mn$_{1.5}$O$_4$ cathode.[17,18] In general, surface modification and metal-ion doping for the LiNi$_{0.5}$Mn$_{1.5}$O$_4$ cathode are

[a]*College of Materials and Metallurgy, Guizhou University, Guiyang 550025, China. E-mail: jqli@gzu.edu.cn; jianbing.guo@126.com*

[b]*School of Materials and Metallurgical Engineering, Guizhou Institute of Technology, Guiyang 550003, China*

[c]*National Engineering Research Center for Compounding and Modification of Polymer Materials, Guiyang, 550014, China*

[d]*Guizhou Material Industrial Technology Institute, Material Technology Innovation Base of Guizhou Province, Guiyang, 550014, China*

effective methods to solve this problem.[19–22] In previous studies, cationic doping with Cr,[23] Fe,[24] Cu,[25] Si,[6] Mg,[26] Zr,[27] and Al[28] has been used to eliminate this problem. Although this method improves the cycle lifetime and safety of lithium batteries, it cannot solve the relatively low intrinsic conductivity of $LiNi_{0.5}$-$Mn_{1.5}O_4$ that restricts the capacity of the battery at high rates. The doping of Ru transition metal ion in $LiNi_{0.5}Mn_{1.5}O_4$ is an effective method to solve this problem.[29] Compared with the 3d orbital, the Ru 4d orbital with a larger radius of the second-row transition metal ions overlapping with the 2p orbital of oxygen favors wider conduction bands.[30] Moreover, the study of improving the electrochemical properties of LNMO *via* different synthesis techniques to achieve Ru doping is still under continuous exploration and improvement. Wang *et al.*[31,32] prepared an Ru-doped LNMO cathode electrode *via* a solid-state reaction and polymer-assisted method to improve the electro-chemical performance of the material. Chae *et al.*[33] prepared Ru doped LNMO cathode materials *via* the carbon combustion method, and explored the influence of Ru doping on the material structure and composition charges. Although the solid-state method and combustion method are simple, the particle of the cathode sample is not uniformly distributed and easily agglom-erates. In contrast, the cathode sample prepared *via* the hydro-thermal method has better particle dispersion, higher particle purity and lower production cost, which are beneficial to obtaining a cathode with excellent discharge capacity and cycle stability.[34] Investigating through numerous reports, a few were found on the Ru-doped LNMO cathode prepared *via* a mild and simple hydro-thermal synthesis method.

In this study, different amounts of Ru doping $LiNi_{0.5}Mn_{1.5}O_4$ cathode materials have been prepared by a simple hydro-thermal reaction. The crystal structure, morphology, charge–discharge capacity, cycle, and rate performance of the $LiMn_{1.5}Ni_{0.5-x}Ru_xO_4$ ($x = 0$, 0.02, 0.04, and 0.06) cathode have been explored. The results reveal that Ru doping can effectively inhibit the formation of impure phases and maintain electrical property stability at high current density, useful for preparing lithium-ion batteries with desirable performance.

2. Experimental

2.1. Material synthesis

Mn $(CH_3COO)_2 \cdot 4H_2O$, Ni $(CH_3COO)_2 \cdot 4H_2O$ and RuO_2 of analytical grade were purchased from Aladdin Bio-Chem Technology Co., Ltd, and Li_2CO_3 and NH_4HCO_3 were purchased Tianjin Yongda Chemical Reagent Co. Ltd. All reagents were used without further purification. The $LiMn_{1.5}$-$Ni_{0.5-x}Ru_xO_4$ ($x = 0$, 0.02, 0.04, and 0.06) cathodes were synthesized *via* a hydrothermal method.

In a typical synthesis process, Li_2CO_3 (0.025 mol), $Mn(CH_3\text{-}COO)_2$ (0.075 mol), $Ni(CH_3COO)_2$ (0.025, 0.024, 0.023, and 0.022 mol) and RuO_2 (0, 0.001, 0.002, and 0.003) were dissolved in 90 mL deionized water to obtain a mixture solution A. Simul-taneously, NH_4HCO_3 (7.906 g) was dissolved in 20 mL of deionized water and stirred under 10 °C to obtain solution B. Then, the solution B was added dropwise into the solution A, and the mixture was stirred vigorously to obtain a homogeneous

mixture solution. The as-obtained solution was transferred into a high pressure reactor and kept at 190 °C for 24 h. After drying at 90 °C for 12 h, the samples were ground for 2 h. Then, the as-obtained mixture was synthesized to obtain the $LiMn_{1.5}$-$Ni_{0.5-x}Ru_xO_4$ cathode according to the following procedure: (1) sintering at 650 °C for 5 h; (2) ramping to 850 °C, sintering for 12 h; (3) cooling to 600 °C isothermal for 2 h. The as-prepared samples were named Ru-0, Ru-2, Ru-4 and Ru-6, respectively.

2.2. Material characterization

A Fourier transform infrared spectrometer (Thermo Scientific Nicolet Is50) was used to characterize the ordered and disor-dered structure fd the material. The crystal structure was studied by X-ray diffraction (Bruker D8 Advance) using Cu Kα radiation. The scanning rate was $10° \text{ min}^{-1}$ in $2\theta = 10\text{--}80°$. The morphologies and particle size images, EDS spectra, and mapping images were obtained *via* field emission scanning electron microscopy (Zeiss Merlin Compact). The particle size distribution curves of all samples were tested using the laser particle size distribution analyzer (Bettersize 2600). The valences of Ni, Mn, C, and Ru elements on the sample surface were measured *via* X-ray photoelectron spectroscopy (Thermo Scientific K-Alpha) using Al Kα radiation.

2.3. Electrochemical measurements

The active materials 80 wt%, conductive carbon black 10 wt%, and polyvinylidene fluoride (PVDF) 10 wt% were evenly mixed and *N*-methyl-2-pyrrolidone (NMP) was added to the mixture to obtain a slurry solution. The slurry was coated on an Al foil and dried at 80 °C overnight in a vacuum.[35] Through slicing, the cathode pole piece is obtained. Lithium was used as the anode. 1 M $LiPF_6$ was dissolved in a mixed solution of diethyl carbonate (DEC), and ethylene carbonate (EC) (volume ratio of 1 : 1) to obtain the electrolyte. The CR-2032 type coin cells were assembled in a glove box filled with argon. The charge/discharge tests were conducted on an automatic galvanostatic charge–discharge tester (NEWARE) at different rates (1C = 200 mA g^{-1}). Electrochemical impedance spectroscopy (EIS) was carried out on an electrochemical workstation (CHI 760E) in a frequency range of 100 000–0.01 Hz. All coin cells were tested at room temperature.

3. Results and discussion

3.1. Structure and morphology

It is well known that $LiNi_{0.5}Mn_{1.5}O_4$ has two space group structures, according to the Ni/Mn disordered face-centered cubic structure ($Fd\bar{3}m$ space group) and Ni/Mn ordered simple cubic structure ($P4_332$ space group). The crystal structure has a great influence on the electrochemical performance on the cathode. FTIR spectroscopy is used to identify the disordered or ordered structures of spinel $LiNi_{0.5}Mn_{1.5}O_4$. Fig. 1 shows the FTIR spectra of Ru-0, Ru-2, Ru-4, and Ru-6. The spectrum of each sample is similar. The obvious peaks at 620 cm^{-1} and 584 cm^{-1} correspond to Mn–O and Ni–O bands, respectively.[36] For all the samples, the Mn–O peak located at 620 cm^{-1} is
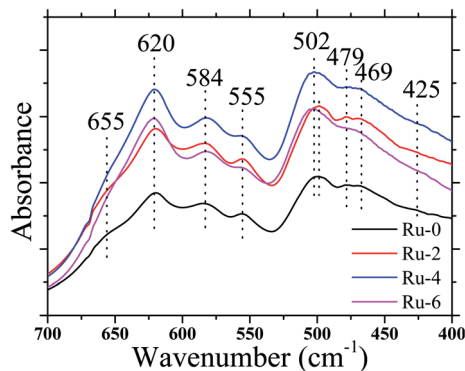
Fig. 1 FTIR spectra of LiMn$_{1.5}$Ni$_{0.5-x}$Ru$_x$O$_4$ (x = 0, 0.02, 0.04, and 0.06) samples.

Fig. 2 XRD patterns of LiMn$_{1.5}$Ni$_{0.5-x}$Ru$_x$O$_4$ (x = 0, 0.02, 0.04, and 0.06) samples.

higher than the Ni–O peak located at 584 cm^{-1}, indicating the existence of the disordered $Fd\bar{3}m$ space group.[37] However, for Ru-0 and Ru-2, they also show weak peaks at around 655 cm^{-1}, which is a characteristic of the $P4_332$ space group structure.[38] Moreover, there is no obvious absorption peak at 425 cm^{-1}, indicating that there is a weak ordered $P4_332$ structure in those samples. However, with the further incorporation of Ru, the disappearance of the peak at 655 cm^{-1} indicates that the ordered structure of the material was further transformed into a disordered structure. In addition, the strength ratios of the Mn–O peak at 620 cm^{-1} and Ni–O peak at 584 cm^{-1} are 1.10, 1.10, 1.15 and 1.20, respectively, which further indicate that the disorder of the material is higher with the continuous addition of Ru.[39] Therefore, according to the FTIR analysis, the hydrothermal synthesis samples are all disordered $Fd\bar{3}m$ space group structure that contained slightly ordered $P4_332$ space group structure, and the ordered $P4_332$ space group structure
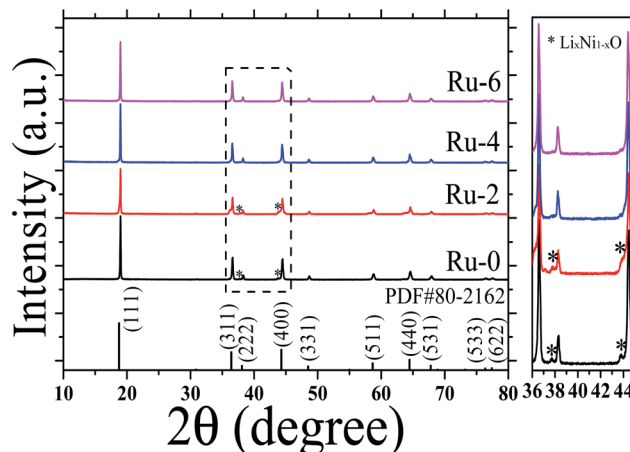
continues to decrease with the increase in the Ru ion addition. It is well known that LiNi$_{0.5}$Mn$_{1.5}$O$_4$ of the disordered $Fd\bar{3}m$ space group structure has better electrochemical performance than the LiNi$_{0.5}$Mn$_{1.5}$O$_4$ of $P4_332$ space group structure. Therefore, the addition of Ru may be beneficial to improve the electrochemical performance of the material.

To study the crystal structure of the Ru-doped LiMn$_{1.5}$Ni$_{0.5}$O$_4$ materials, the XRD patterns of the LiMn$_{1.5}$Ni$_{0.5-x}$Ru$_x$O$_4$ (x = 0, 0.02, 0.04, and 0.06) samples were analyzed, as shown in Fig. 2. The sharp diffraction peaks indicate that all the samples have good crystallinity. According to the FTIR analysis, all samples belong to the $Fd\bar{3}m$ space group, and XRD also shows that all samples conform to the spinel LiMn$_{1.5}$Ni$_{0.5}$O$_4$ standard card (PDF# 80-2162). The doping of Ru has no obvious effect on the

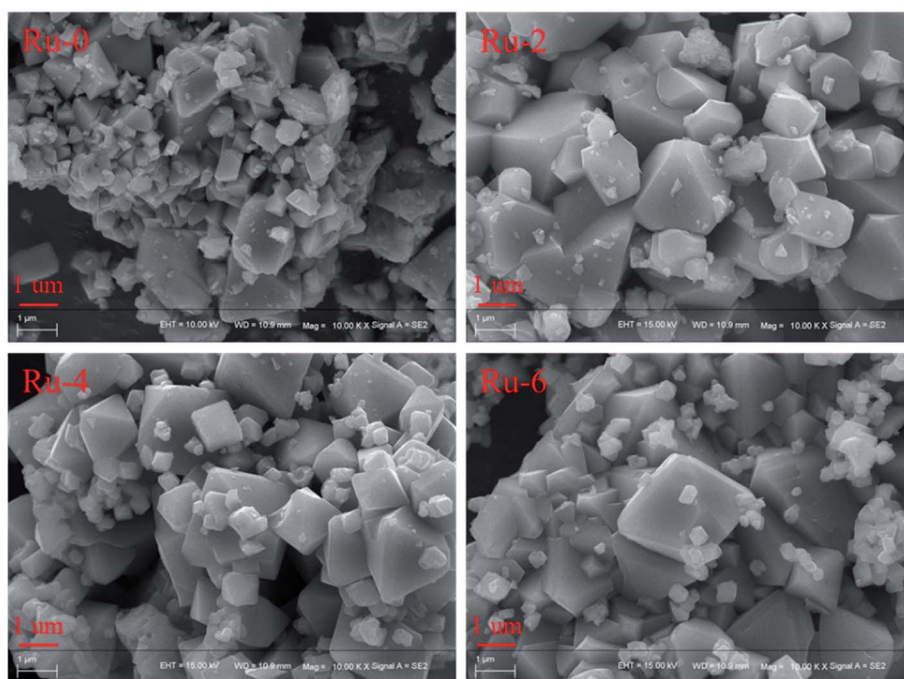**Fig. 3** The SEM images of LiMn$_{1.5}$Ni$_{0.5-x}$Ru$_x$O$_4$ (x = 0, 0.02, 0.04, and 0.06) samples with different Ru-doped contents.

lattice frame of $LiMn_{1.5}Ni_{0.5}O_4$, and there is no RuO_2 phase detected in the samples. However, the Ru-0 and Ru-2 samples have weak diffraction peaks at about 37.6, 43.6, and 63.5°, which are attributed to the $Li_xNi_{1-x}O$ impurity phase structure.[33] With the further doping of Ru, the $Li_xNi_{1-x}O$ impurity phase structure in Ru-4 and Ru-6 samples disappeared. The results reveal the doped Ru ions did not destroy the cubic spinel crystal structure of the $LiMn_{1.5}Ni_{0.5}O_4$, and can inhibit the formation of an impurity phase, thus stabilizing the cubic spinel crystal structure.

The morphology and size of the material have important influence on the electrochemical performance.[40–42] The SEM images of each sample are shown in Fig. 3. It can be seen from the SEM images that all samples are composed of octahedral-like particles with good crystallinity. The particle sizes of the samples are about 2 μm with numerous nanoparticles attached on the surface. With the addition of Ru, smaller octahedral particles dispersed in the sample, and there are obvious boundaries between particles, which should be because the addition of the Ru source in the sintering process hinders the growth of the cathode material particles.[33]

In order to further verify the influence of Ru doping on the particle size distribution of the samples, the particle size distribution curves of all the samples are shown in Fig. 4. It can be observed from Fig. 4 that the D50 value of all the samples is basically around 2 μm, and with the doping of Ru, the D50 value of the samples decreases by about 3.5 μm. This result is consistent with the SEM analysis of the effects of Ru doping on the particle size of the material.

In order to further detect the composition of Ru-doped samples and original samples, EDS spectra and element distribution images of undoped and Ru-doped samples are shown in Fig. 5. It can be clearly seen from the EDS spectrum that the undoped sample only has characteristic peaks of Mn, Ni and O. However, Ru-doped samples with Ru ions doped can have obvious Ru characteristic peaks in EDS spectra. This indicates that Ru ions have been incorporated into the cathode material. It is observed from the elemental distribution diagram that O, Ni and Mn in samples are evenly distributed in each material and present a good distribution.

Fig. 6 shows the XPS spectra of the doped and undoped samples. Fig. 6a showed that all samples were composed of Ni, Mn, O, C and Li, and the Ru element was not detected due to its low content. The scanning spectrum of Ru 3p is represented in Fig. 6b to better characterize the existence of the Ru element. Two distinct diffraction peaks around 486 and 464 eV are observed corresponding to Ru $3p_{1/2}$ and Ru $3p_{3/2}$, which confirm the existence of Ru.[43] Moreover, with the increase in the Ru content, the diffraction peaks of Ru 3p gradually increase. The peak around 281.5 eV in Fig. 6c also confirms the presence of Ru^{4+}.[33] Mn ions exist in the form of Mn^{3+} and Mn^{4+} in the $Fd\bar{3}m$ space group structure. Fig. 6d shows two distinct diffraction peaks located at 654 and 642 eV, corresponding to Mn $2p_{1/2}$ and Mn $2p_{3/2}$. The fitting peaks for the Mn $2p_{3/2}$ peak observed at 643.2 and 641.8 eV are attributed to Mn^{4+} and Mn^{3+}, respectively.[39] According to the peak-splitting fitting, the proportions of Mn^{3+}/Mn^{4+} in Ru-0, Ru-2, Ru-4, and Ru-6 samples were 65.32 : 34.68, 65.56 : 34.44, 65.70 : 34.30, and 66.37 : 34.63,

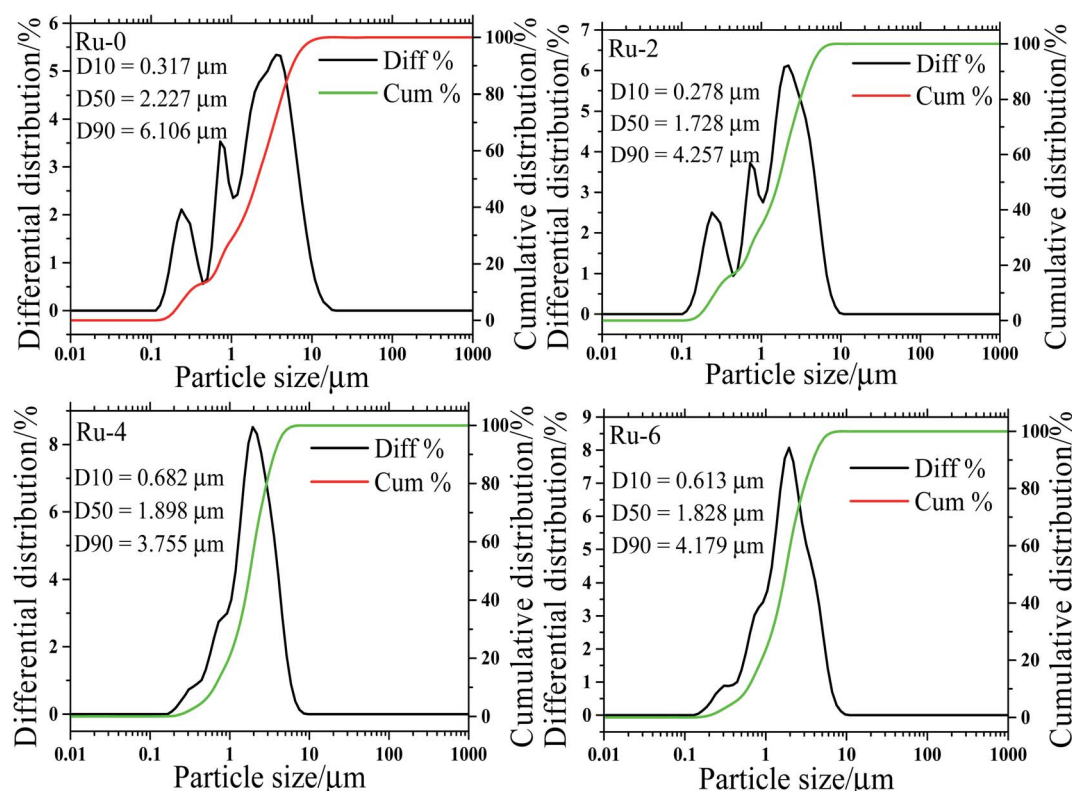**Fig. 4** The particle size distribution diagram of $LiMn_{1.5}Ni_{0.5-x}Ru_xO_4$ (x = 0, 0.02, 0.04, and 0.06) samples with different Ru-doped contents.

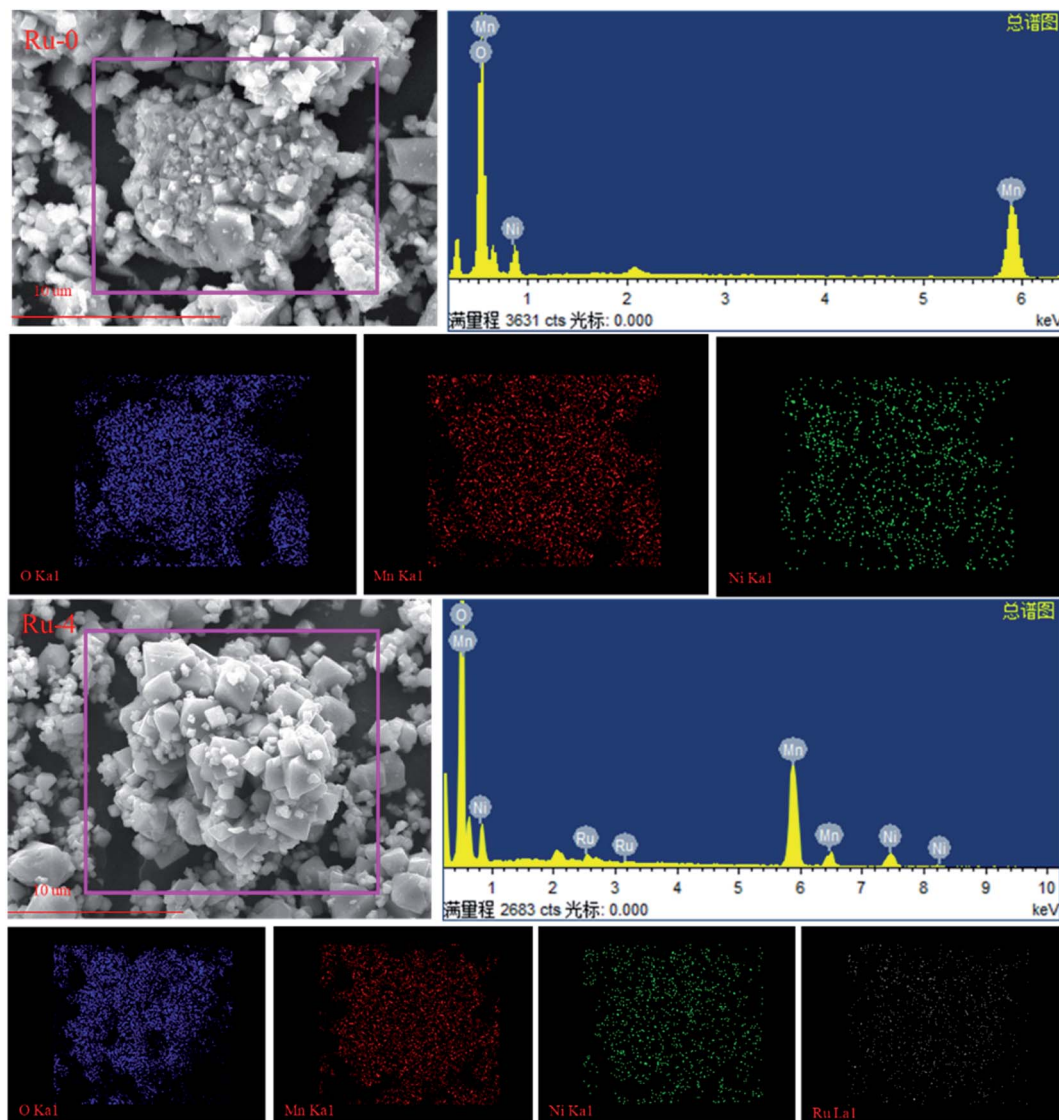**Fig. 5** The EDS spectra and element mapping of $LiMn_{1.5}Ni_{0.5-x}Ru_xO_4$ ($x = 0$ and 0.04) samples.

respectively. It can be seen that with the increase in doped Ru, the content of Mn^{3+} in the sample also increases gradually. This may be due to the addition of Ru^{4+} ions induce to part of Mn^{4+} transfer to Mn^{3+} to balance the charge. More Mn^{3+} ions in the material can improve the electrical conductivity of the material.[44] This is also consistent with the results of the FTIR analysis that the structure of the disordered $Fd\bar{3}m$ space group increases with the increase in the Ru content.

3.2. Electrochemical properties

The galvanostatic charge and discharge capacity, cycling stability, and rate performance were measured to examine the electrochemical performance of LNMO cathode materials with different Ru doping contents. Fig. 7 presents the first three charge–discharge capacity curves of Ru-0, Ru-2, Ru-4, and Ru-6 samples measured between 3.0 and 4.9 V at a rate of 0.25C, in which a dominating charge plateau around 4.7 V corresponds to

Ni^{2+}/Ni^{3+} and Ni^{3+}/Ni^{4+} redox couples and a weak plateau at about 4 V is attributable to the Mn^{3+}/Mn^{4+} redox couple.[33] During the first charge/discharge process, the Ru-0 sample showed a lower charge/discharge specific capacity (97.63/ 93.64 mA h g^{-1}). While Ru doped samples show a high charge and discharge specific capacity. The Ru-4 sample shows a higher initial charge/discharge specific capacity (139.49/ 140.16 mA h g^{-1}) and the highest coulomb efficiency (~100%). This is attributed to the Ru doping. On the one hand, Ru doping hinders the growth of positive particles and shortens the diffusion path of lithium ions. On the other hand, the Ru doping inhibits the formation of $Li_xNi_{1-x}O$ impurity and expands the diffusion path of lithium ions.[33]

According to the charge–discharge curve analysis, the doping of Ru ions can improve the specific discharge capacity of the spinel cathode. To compare the charge–discharge rate performance of Ru-doped samples and the original sample, the charge–discharge specific capacity of all samples was tested at
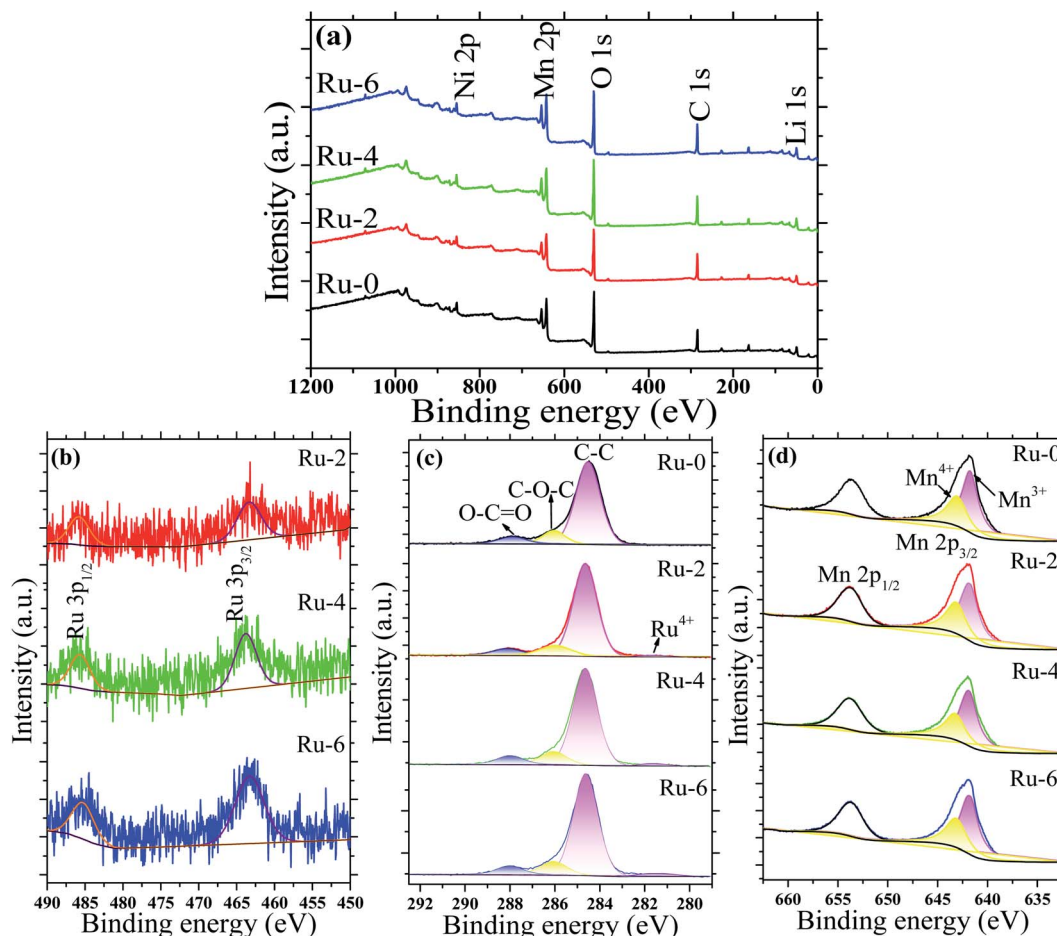
Fig. 6 The XPS spectra of LiMn$_{1.5}$Ni$_{0.5-x}$Ru$_x$O$_4$ (x = 0, 0.02, 0.04, and 0.06) samples: (a) XPS survey spectrogram; (b) Ru 3p spectrogram; (c) C 1s spectrogram; and (d) Mn 2p spectrogram.

different current densities of 0.25C to 5C, as shown in Fig. 8a. With the increase in the current density, the discharge specific capacity of all the samples shows a gradual decreasing trend, which is considered to be a result of the increase in battery polarization with the increase in the current density.[33] The Ru-doped samples have higher discharge specific capacity than the original samples at different discharge rates. It is worth noting that the discharge specific capacity of the Ru-4 sample is about 10 mA h g^{-1} higher than that of the Ru-6 sample at a current density below 2.5C. The decisive factor of capacity is the particle size at low current density, and the small particle size is beneficial to lithium-ion diffusion to obtain a high discharge capacity. The D90 of the Ru-4 sample is 3.755 μm, which is smaller than that of the Ru-6 sample (D90, 4.179 μm), so the Ru-4 owns higher capacity. While the current density surpasses 2.5C, the discharge specific capacity of the Ru-6 sample is about 10 mA h g^{-1}, which is higher than that of the Ru-4 sample. This is because the charge transfer resistance (R_{ct}) is dominant for the discharge capacity at larger currents. The R_{ct} of the Ru-6 sample is lower than that of the Ru-4 sample, as shown in Table 2. Therefore, the capacity of Ru-6 is bigger than that of Ru-4 at high current density. According to the analysis above, small amounts of Ru element doping can improve the rate capacity of

the spinel cathode material at low current density; however, the rate capacity of materials will be improved at a high current density with the further increase in the content of Ru. This may be because the incorporation of Ru ions expands the diffusion channel of lithium ions and is more conducive to the embedding and exiting of lithium ions.

Fig. 8b shows the discharge capacity of all samples at different cycling numbers at a discharge rate of 1C. It is shown that the discharge specific capacities of Ru-4 and Ru-6 are about 30 mA h g^{-1} higher than that of the original sample, while the discharge specific capacity of the slightly Ru-doped Ru-4 sample is not much different from that of the original sample. This may be due to the influence of the Li$_x$Ni$_{1-x}$O impurity phase and a small amount of the ordered $P4_332$ space group structure in Ru-0 and Ru-2 samples. In the first few cycles, the discharge specific capacity of the original sample is low; however, the discharge specific capacity of the Ru-doped sample basically reached the maximum value, and this stage belongs to the activation stage of the battery. The specific discharge capacity of Ru-doped samples is basically stable in the early stage, which may be related to the fact that Ru doping shortens the lithium ion diffusion path and expands the lithium ion diffusion channel. In order to better show the influence of Ru doping on
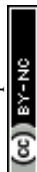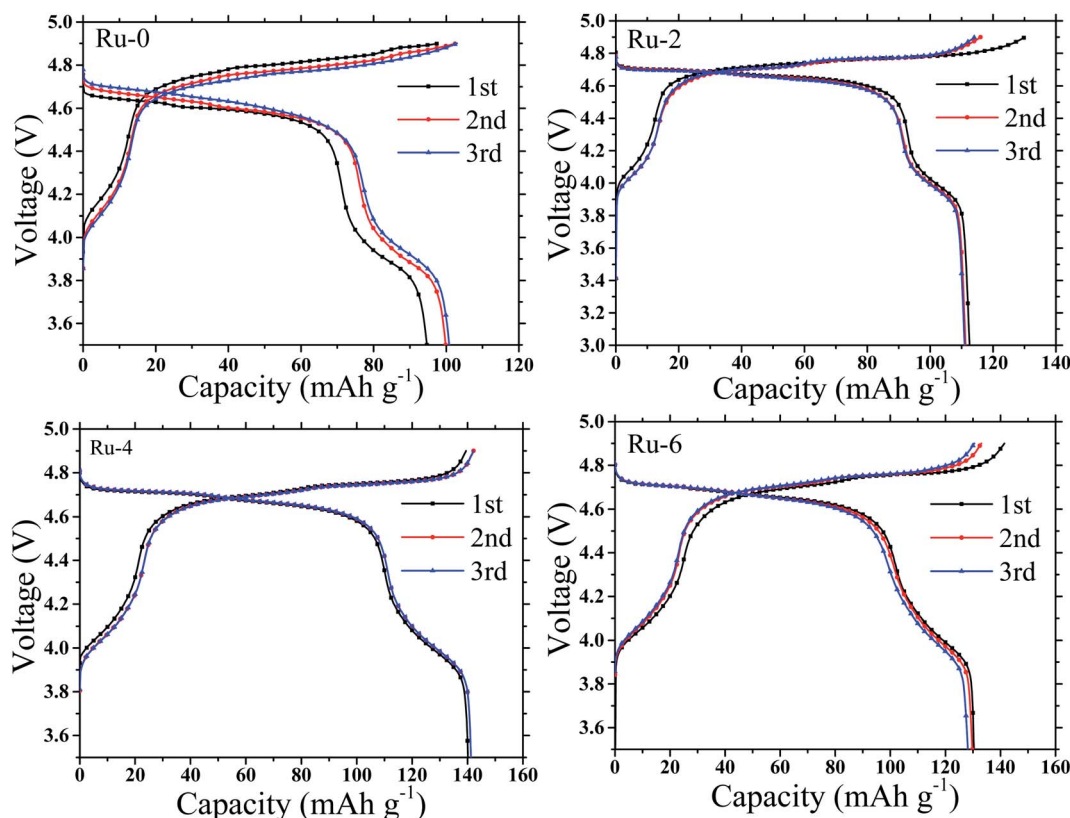
Fig. 7 The galvanostatic charging and discharging curve of LiMn$_{1.5}$Ni$_{0.5-x}$Ru$_x$O$_4$ (x = 0, 0.02, 0.04, and 0.06) samples at 0.25C.

the electrochemical properties of materials, the initial discharge specific capacity, maximum discharge specific capacity, final discharge specific capacity and capacity retention of each sample are shown in Table 1. It can be seen from Table 1 that Ru doping not only improves the specific discharge capacity of the material, but also improves the cyclic stability of the material. In particular, the discharge specific capacities of Ru-4 and Ru-6 samples are about 30 mA h g^{-1} higher than that of the original samples, and the capacity retention rates of Ru-4 and Ru-6 samples are 97.82 and 99.86% after 100 cycles, respectively, which are higher than that of the original samples (95.39%). Therefore, it can be seen that Ru ion doping not only

improves the specific charge–discharge capacity of the material but also improves the cyclic stability of the material, which should not only be related to the fact that Ru ion doping enlarges the diffusion channel and shortens the diffusion path of lithium ions, but also may be related to the strong TM-O hybridization of 4d transition metal (TM) ions.

Fig. 9 shows the EIS spectra of Ru-0, Ru-2, Ru-4, and Ru-6 after 100 cycles and corresponding equivalent circuit. The EIS curves after the cycle are all composed of a semicircle in the middle and high frequency regions, and a straight line in the low frequency region. The high-frequency and low-frequency semicircles represent the interface resistance (R_f) of lithium-
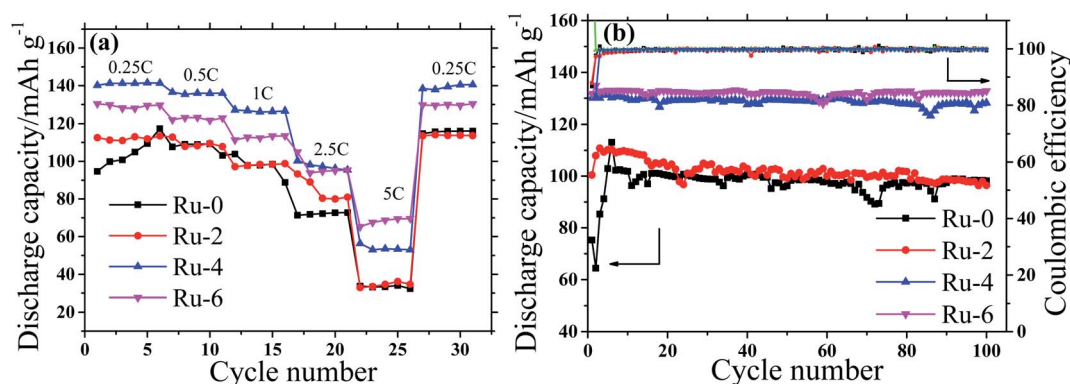

Fig. 8 The rate capacity and cycle stability of the LiMn$_{1.5}$Ni$_{0.5-x}$Ru$_x$O$_4$ (x = 0, 0.02, 0.04, and 0.06) cathodes (a) rate capability, (b) cycle performance.

Table 1 The initial discharge specific capacity, maximum discharge specific capacity, final discharge specific capacity and capacity retention of Ru-0, Ru-2, Ru-4, and Ru-6 samples

	Discharge capacity (mA h g^{-1})			Capacity retention ratio
Samples	1st	Maximum	100th	
Ru-0	75.32	102.92	98.18	95.39%
Ru-2	100.42	110.78	96.42	87.04%
Ru-4	130.06	131.26	128.15	97.82%
Ru-6	131.68	133.00	132.81	99.86%
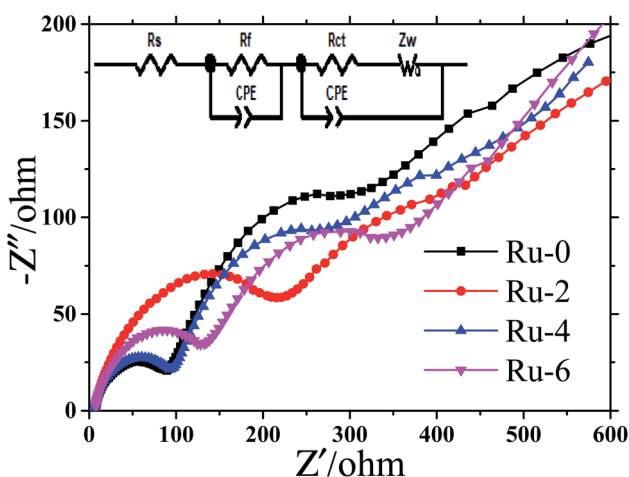
Fig. 9 The EIS spectral of $LiMn_{1.5}Ni_{0.5-x}Ru_xO_4$ ($x = 0$, 0.02, 0.04, and 0.06) samples after 100 cycles and corresponding equivalent circuit.

ion migration through the material and electrolyte interface and R_{ct}, respectively.[45,46] The straight line represents the resistance (Warburg impedance (Z_w)) of lithium ion diffusion in the solid material.[47] According to the fitting results of Nyquist plots, the ohmage (R_s), R_f, and R_{ct} values of all samples are shown in Table 2. It is found from Table 2 that the R_s of the electrode is negligible. The R_f of the Ru-doped material increases slightly, which is caused by the formation and thickening of the SEI film on the surface of the material. This may be because the addition of Ru increases the side reaction between the spinel cathode material and the electrolyte. However, the value of R_{ct} of Ru-doped samples decreases gradually, indicating that Ru doping can reduce the charge transfer impedance. This is the reason for the excellent rate performance of Ru-doped materials.

Table 2 The fitting parameters of $LiMn_{1.5}Ni_{0.5-x}Ru_xO_4$ ($x = 0$, 0.02, 0.04, and 0.06) samples after 100 cycles at 1C

Samples	R_s/Ω	R_f/Ω	R_{ct}/Ω
Ru-0	6.049	80.36	312.5
Ru-2	6.422	187.60	309.8
Ru-4	5.119	85.48	272.9
Ru-6	5.822	129.9	238.8

4. Conclusions

In this study, the spinel cathode materials $LiNi_{0.5}Mn_{1.5}O_4$ with the $Fd\bar{3}m$ space group structure were successfully prepared via a simple hydrothermal reaction, followed by a heat treatment method. All the cathodes have good crystallinity. When Ru was added into $LiNi_{0.5}Mn_{1.5}O_4$, the ordered structure of the cathode decreased, the $Li_xNi_{1-x}O$ impurity phase decreased, and the content of Mn^{3+} ion increased in the cathode, which is conducive to the embedding and de-embedding of lithium ions. The electrochemical performance also further verified that the addition of Ru element not only improved the specific discharge capacity of the material but also improved the cyclic performance and rate performance of the material. Particularly, through the rate performance, it is realized that Ru doping can improve the discharge specific capacity of LNMO cathode materials at high current densities.

Conflicts of interest

There are no conflicts to declare.

Acknowledgements

References

1 H. Wang, T. A. Tan, P. Yang, M. O. Lai and L. Lu, High-Rate Performances of the Ru-Doped Spinel $LiNi_{0.5}Mn_{1.5}O_4$: Effects of Doping and Particle Size, *J. Phys. Chem. C*, 2011, **115**, 6102–6110.

2 S.-T. Myung, K. Amine and Y.-K. Sun, Nanostructured cathode materials for rechargeable lithium batteries, *J. Power Sources*, 2015, **283**, 219–236.

3 L. H. Saw, Y. Ye and A. A. O. Tay, Integration issues of lithium-ion battery into electric vehicles battery pack, *J. Cleaner Prod.*, 2016, **113**, 1032–1045.

4 Y. Luo, H. Li, T. Lu, Y. Zhang, S. S. Mao, Z. Liu, W. Wen, J. Xie and L. Yan, Fluorine gradient-doped $LiNi_{0.5}Mn_{1.5}O_4$ spinel with improved high voltage stability for Li-ion batteries, *Electrochim. Acta*, 2017, **238**, 237–245.

5 J. W. Fergus, Recent developments in cathode materials for lithium ion batteries, *J. Power Sources*, 2010, **195**, 939–954.

6 B. Zong, Z. Deng, S. Yan, Y. Lang, J. Gong, J. Guo, L. Wang and G. Liang, Effects of Si doping on structural and electrochemical performance of $LiNi_{0.5}Mn_{1.5}O_4$ cathode materials for lithium-ion batteries, *Powder Technol.*, 2020, **364**, 725–737.

7 M. S. Whittingham, Lithium batteries and cathode materials, *Chem. Rev.*, 2004, **104**, 4271–4301.

8 J. Zhang, G. Sun, Y. Han, F. Yu, X. Qin, G. Shao and Z. Wang, Boosted electrochemical performance of LiNi$_{0.5}$Mn$_{1.5}$O$_4$ via synergistic modification of Li$^+$-Conductive Li$_2$ZrO$_3$ coating layer and superficial Zr-doping, *Electrochim. Acta*, 2020, **343**, 136105.

9 A. Ulvestad, J. N. Clark, O. G. Shpyrko, A. Singer, Y. S. Meng, H. M. Cho, R. Harder, J. Maser and J. W. Kim, Topological defect dynamics in operando battery nanoparticles, *Science*, 2015, **348**, 1344–1347.

10 D. W. Kim, H. Shiiba, N. Zettsu, T. Yamada, T. Kimijima, G. Sánchez-Santolino, R. Ishikawa, Y. Ikuhara and K. Teshima, Full picture discovery for mixed-fluorine anion effects on high-voltage spinel lithium nickel manganese oxide cathodes, *NPG Asia Mater.*, 2017, **9**, 1–10.

11 G. Li, S. Zhou, P. Wang and J. Zhao, Halogen-doping in LiCoO2 cathode materials for Li-ion batteries: insights from *ab initio* calculations, *RSC Adv.*, 2015, **5**, 107326–107332.

12 S. H. Kim and C.-S. Kim, Improving the rate performance of LiCoO$_2$ by Zr doping, *J. Electroceram.*, 2009, **23**, 254–257.

13 A. Manthiram, K. Chemelewski and E.-S. Lee, A perspective on the high-voltage LiMn$_{1.5}$Ni$_{0.5}$O$_4$ spinel cathode for lithium-ion batteries, *Energy Environ. Sci.*, 2014, **7**, 1339–1350.

14 R. Amin and I. Belharouk, Part I: Electronic and ionic transport properties of the ordered and disordered LiNi$_{0.5}$Mn$_{1.5}$O$_4$ spinel cathode, *J. Power Sources*, 2017, **348**, 311–317.

15 L. Wang, H. Li, X. Huang and E. Baudrin, A comparative study of Fd-3m and P4$_3$32 "LiNi$_{0.5}$Mn$_{1.5}$O$_4$", *Solid State Ionics*, 2011, **193**, 32–38.

16 M. Bini, P. Boni, P. Mustarelli, I. Quinzeni, G. Bruni and D. Capsoni, Silicon-doped LiNi$_{0.5}$Mn$_{1.5}$O$_4$ as a high-voltage cathode for Li-ion batteries, *Solid State Ionics*, 2018, **320**, 1–6.

17 W. Li, Y.-G. Cho, W. Yao, Y. Li, A. Cronk, R. Shimizu, M. A. Schroeder, Y. Fu, F. Zou, V. Battaglia, A. Manthiram, M. Zhang and Y. S. Meng, Enabling high areal capacity for Co-free high voltage spinel materials in next-generation Li-ion batteries, *J. Power Sources*, 2020, **473**, 228579.

18 H. Xu, H. Zhang, J. Ma, G. Xu and G. Cui, Overcoming the challenges of 5 V spinel LiNi$_{0.5}$Mn$_{1.5}$O$_4$ cathodes with solid polymer electrolytes, *ACS Energy Lett.*, 2019, **4**, 2871–2886.

19 Q. Wu, X. Zhang, S. Sun, N. Wan, D. Pan, Y. Bai, H. Zhu, Y. Hu and S. Dai, Improved electrochemical performance of spinel LiMn$_{1.5}$Ni$_{0.5}$O$_4$ through MgF$_2$ nano-coating, *Nanoscale*, 2015, **7**, 15609–15617.

20 H. Deng, P. Nie, H. Luo, Y. Zhang, J. Wang and X. Zhang, Highly enhanced lithium storage capability of LiNi$_{0.5}$Mn$_{1.5}$O$_4$ by coating with Li$_2$TiO$_3$ for Li-ion batteries, *J. Mater. Chem. A*, 2014, **2**, 18256–18262.

21 S. Li, W. Liang, J. Xie, Y. Wei and X. Cui, Synthesis of hollow microspheres LiNi$_{0.5}$Mn$_{1.5}$O$_4$ coated with Al$_2$O$_3$ and characterization of the electrochemical capabilities, *J. Electrochem. Energy Convers. Storage*, 2020, **17**, 031007.

22 Y. Yang, S. Li, Q. Zhang, Y. Zhang and S. Xu, Spherical agglomeration of octahedral LiNi$_{0.5}$Co$_{4x}$Mn$_{1.5-3x}$O$_4$ cathode material prepared by a continuous coprecipitation

method for 5V lithium-ion batteries, *Ind. Eng. Chem. Res.*, 2017, **56**, 175–182.

23 J. Wang, P. Nie, G. Xu, J. Jiang, Y. Wu, R. Fu, H. Dou and X. Zhang, High-voltage LiNi$_{0.45}$Cr$_{0.1}$Mn$_{1.45}$O$_4$ cathode with superlong cycle performance for wide temperature lithium-ion batteries, *Adv. Funct. Mater.*, 2018, **28**, 1704808.

24 Y. Mu, M. Zeng, X. Wu and X. Tong, Electrochemical performance of LiFe$_x$Ni$_{0.5-x}$Mn$_{1.5}$O$_4$ cathode material for lithium-ion batteries, *Int. J. Electrochem. Sci.*, 2017, **12**, 6045–6053.

25 H. Sun, X. Kong, B. Wang, T. Luo and G. Liu, Cu doped LiNi$_{0.5}$Mn$_{1.5-x}$Cu$_x$O$_4$ (x = 0, 0.03, 0.05, 0.10, 0.15) with significant improved electrochemical performance prepared by a modified low temperature solution combustion synthesis method, *Ceram. Int.*, 2018, **44**, 4603–4610.

26 M. Liu, H. Huang, C. Lin, J. Chen and S. Liao, Mg gradient-doped LiNi$_{0.5}$Mn$_{1.5}$O$_4$ as the cathode material for Li-ion batteries, *Electrochim. Acta*, 2014, **120**, 133–139.

27 S. Feng, X. Kong, H. Sun, B. Wang, T. Luo and G. Liu, Effect of Zr doping on LiNi$_{0.5}$Mn$_{1.5}$O$_4$ with ordered or disordered structures, *J. Alloys Compd.*, 2018, **749**, 1009–1018.

28 Y. Luo, T. Lu, Y. Zhang, L. Yan, S. Mao and J. Xie, Surface-segregated, high-voltage spinel lithium-ion battery cathode material LiNi$_{0.5}$Mn$_{1.5}$O$_4$ cathodes by aluminium doping with improved high-rate cyclability, *J. Alloys Compd.*, 2017, **703**, 289–297.

29 J. Liu and A. Manthiram, Understanding the Improved Electrochemical Performances of Fe-Substituted 5 V Spinel Cathode LiMn$_{1.5}$Ni$_{0.5}$O$_4$, *J. Phys. Chem. C*, 2009, **113**, 15073–15079.

30 H. Matsumoto, D. Murakami, T. Shimura, S.-I. Hashimoto and H. Iwahara, Mixed electronic-ionic conduction in Ru-doped SrTiO$_3$ at high temperature, *J. Electroceram.*, 2001, **7**, 107–111.

31 H. Wang, H. Xia, M. O. Lai and L. Lu, Enhancements of rate capability and cyclic performance of spinel LiNi$_{0.5}$Mn$_{1.5}$O$_4$ by trace Ru-doping, *Electrochem. Commun.*, 2009, **11**(7), 1539–1542.

32 H. Wang, T. Tan, P. Yang, M. Lai and L. Lu, High-rate performances of the Ru-doped spinel LiNi$_{0.5}$Mn$_{1.5}$O$_4$: Effects of doping and particle size, *J. Phys. Chem. C*, 2011, **115**, 6102–6110.

33 J. Chae, M. Jo, Y.-I. Kim, D.-W. Han, S.-M. Park, Y.-M. Kang and K. Roh, Kinetic favorability of Ru-doped LiNi$_{0.5}$Mn$_{1.5}$O$_4$ for high-power lithium batteries, *J. Ind. Eng. Chem.*, 2015, **21**, 731–735.

34 T. Zhao, X. Gao, Z. Wei, K. Guo, F. Wu, L. Li and R. Chen, Three-dimensional Li$_{1.2}$Ni$_{0.2}$Mn$_{0.6}$O$_2$ cathode materials synthesized by a novel hydrothermal method for lithium-ion batteries, *J. Alloys Compd.*, 2018, **757**, 16–23.

35 S. Khateeb, A. Lind, R. Santos-Ortiz, N. Shepherd and K. Jones, Effects of steel cell components on overall capacity of pulsed laser deposited FeF$_2$ thin film lithium ion batteries, *J. Electrochem. Soc.*, 2015, **162**, A1667–A1674.

36 L. Wang, H. Li, X. Huang and E. Baudrin, A comparative study of Fd-3m and P4$_3$32 "LiNi$_{0.5}$Mn$_{1.5}$O$_4$", *Solid State Ionics*, 2011, **193**, 32–38.

37 H. Fang, L. Li and G. Li, A Low-temperature Reaction Route to High Rate and High Capacity $LiNi_{0.5}Mn_{1.5}O_4$, *J. Power Sources*, 2007, **167**(1), 223–227.

38 D. Li, A. Ito, K. Kobayakawa, H. Noguchi and Y. Sato, Electrochemical characteristics of $LiNi_{0.5}Mn_{1.5}O_4$ prepared by spray drying and post-annealing, *Electrochim. Acta*, 2007, **52**, 1919–1924.

39 A. Wei, W. Li, Q. Chang, X. Bai, R. He, L. Zhang, Z. Liu and Y. Wang, Effect of Mg^{2+}/F^- co-doping on electrochemical performance of $LiNi_{0.5}Mn_{1.5}O_4$ for 5 V lithium-ion batteries, *Electrochim. Acta*, 2019, **323**, 134692.

40 S. Al-Khateeb, A. Lind, R. Santos-Ortiz, N. Shepherd and K. S. Jones, Cycling performance and morphological evolution of pulsed laser-deposited FeF_2 thin film cathodes for Li-ion batteries, *J. Mater. Sci.*, 2015, **50**, 5174–5182.

41 S. Al-Khateeb and T. Sparks, Spray pyrolysis of conductor- and binder-free porous FeS_2 films for high-performance lithium ion batteries, *J. Mater. Sci.*, 2019, **54**, 4089–4104.

42 S. Al-Khateeb and T. Sparks, Pore-graded and conductor- and binder-free FeS_2 films deposited by spray pyrolysis for high-performance lithium-ion batteries, *J. Mater. Res.*, 2019, **34**, 2456–2471.

43 G. Mao, W. Yu, Q. Zhou, L. Li, Y. Huang, Y. Yao, D. Chu, H. Tong and X. Guo, Improved electrochemical performance of high-nickel cathode material with electronic conductor RuO_2 as the protecting layer for lithium-ion batteries, *Appl. Surf. Sci.*, 2020, **531**, 147245.

44 H. Y. Sun, X. Kong, B. S. Wang, T. B. Luo and G. Y. Liu, $LiNi_{0.5}Mn_{1.45}Zn_{0.05}O_4$ with excellent electrochemical performance for lithium ion batteries, *Int. J. Electrochem. Sci.*, 2017, **12**, 8609–8621.

45 D. Aurbach, B. Markovsky, Y. Talyossef, G. Salitra, H. Kim and S. Choi, Studies of cycling behavior, ageing, and interfacial reactions of $LiNi_{0.5}Mn_{1.5}O_4$ and carbon electrodes for lithium-ion 5-V cells, *J. Power Sources*, 2006, **162**, 780–789.

46 H. Wang, L. Ben, H. Yu, Y. Chen, X. Yang and X. Huang, Understanding the effects of surface reconstruction on the electrochemical cycling performance of the spinel $LiNi_{0.5}Mn_{1.5}O_4$ cathode material at elevated temperatures, *J. Mater. Chem. A*, 2017, **5**, 822–834.

47 D. Arumugam and G. P. Kalaignan, Synthesis and electrochemical characterization of nano-CeO_2-coated nanostructure $LiMn_2O_4$ cathode materials for rechargeable lithium batteries, *Electrochim. Acta*, 2010, **55**, 8709–8716.